第 31 卷第 4 期
2015 年 4 月

无 机 化 学 学 报
CHINESE JOURNAL OF INORGANIC CHEMISTRY

Vol.31 No.4
839-847

联咪唑及其衍生物修饰的多酸基化合物的合成、结构和性质

田爱香*,[1] 侯 雪[1] 孙 娜[2] 肖 茹[1] 应 俊[1]
杨 阳[1] 宁亚莉[1] 李天娇[1] 王秀丽*,[1]
([1]渤海大学化学系,锦州 121000)
([2]河北化工医药职业技术学院化学与环境工程系,石家庄 050026)

摘要:通过使用联咪唑及其衍生物 2 种有机配体在水热条件下合成了 2 个多酸基化合物$[Ag_4(biz)_4][H_2P_2Mo_5O_{23}]\cdot 2H_2O$(**1**)和$[Ag_4(bbiz)_4][HPW^{VI}_{10}W^{V}_{2}O_{40}]$(**2**)(biz=2,2-联咪唑,bbiz=5-丁基-2,2-联咪唑),并通过单晶 X-射线衍射、元素分析和红外光谱对其进行了表征。化合物 **1** 包含双核银簇$[Ag_2(biz)_2]^{2+}$,$[P_2Mo_5O_{23}]^{6-}$多阴离子通过提供端基氧原子连接相邻双核银簇而构筑了一维链结构。在化合物 **2** 中,每个 Keggin 型阴离子提供 4 个桥氧原子来连接 4 个双核银簇$[Ag_2(bbiz)_2]^{2+}$,从而构筑一个二维的层结构。此外,对标题化合物的电化学、光催化以及荧光性能也进行了研究。

关键词:多酸基化合物;2,2-联咪唑;5-丁基-2, 2-联咪唑;电化学性能;光催化性能;荧光性能
中图分类号:O614.122 **文献标识码**:A **文章编号**:1001-4861(2015)04-0839-09
DOI:10.11862/CJIC.114

Syntheses, Structures and Properties of Two POM-based Compounds Modified by Biimidazole and Its Derivative

TIAN Ai-Xiang*,[1] HOU Xue[1] SUN Na[2] XIAO Ru[1] YING Jun[1] YANG Yang[1] NING Ya-Li[1]
LI Tian-Jiao[1] WANG Xiu-Li*,[1]
([1]*Department of Chemistry, Bohai University, Jinzhou, Liaoning* 121000, *China*)
([2]*Department of Chemical and Environmental Engineering, Hebei Chemical & Pharmaceutical Vocational Technology College, Shijiazhuang* 050026, *China*)

Abstract: Through using two kinds of ligands (biimidazole and its derivative), two polyoxometalate-based compounds, $[Ag_4(biz)_4][H_2P_2Mo_5O_{23}]\cdot 2H_2O$ (**1**) and $[Ag_4(bbiz)_4][HPW^{VI}_{10}W^{V}_{2}O_{40}]$ (**2**) (biz=2,2-biimidazole, bbiz=5-butyl-2,2-biimidazole), have been synthesized under hydrothermal conditions and characterized by single-crystal X-ray diffraction, elemental analyses and IR spectra. Compound **1** contains bi-nuclear $[Ag_2(biz)_2]^{2+}$ clusters, which are linked by $[P_2Mo_5O_{23}]^{6-}$ anions through terminal O atoms to construct a 1D chain. In compound **2**, each Keggin anion offers four bridging O atoms to link four bi-nuclear $[Ag_2(bbiz)_2]^{2+}$ clusters and a 2D layer of **2** is constructed. Additionally, the electrochemical, photocatalytic and fluorescent properties of the title compounds have been studied. CCDC: 1027614, **1**; 1027615, **2**.

Key words: POM-based compounds; 2,2-biimidazole; 5-butyl-2,2-biimidazole; electrochemical property; photocatalytic property; fluorescent property

收稿日期:2014-11-10。收修改稿日期:2015-01-22。
国家自然科学基金(No.21101015,21471021,21201021)资助项目。
*通讯联系人。E-mail:tian@bhu.edu.cn; wangxiuli@bhu.edu.cn ;会员登记号:S06N2283M1406(田爱香);S06N6675M1005(王秀丽)。

0 Introduction

Over the past decades, the assembly of metal-organic frameworks(MOFs) has attracted great attention owing to not only their structural diversity but also their remarkable applications[1]. Nowadays, polyoxometalates(POMs) have been regarded as excellent inorganic building blocks to construct POM-based MOFs (POMOFs) due to their discrete structures and promising physical and chemical properties, such as optics, electrochemical activity, gas storage, magnetism and catalysis[2]. Among a wide variety of POM types, classical Keggin anions are commonly used and many Keggin-based compounds have been obtained[3]. Compared with Keggin anions, the Strandberg-type anion owns smaller volume and fewer terminal and bridging O atoms. However, it still can be treated as the appropriate candidates for the construction of POMOFs owing to their higher charges and particular structural features. Up to now, a series of Strandberg-based compounds have been synthesized with some excellent properties[4]. For example, Zhu′s group firstly reported three Strandberg-based compounds acting as efficient catalysts for the organic synthesis[5]. In this work, we chose Keggin and Strandberg anions to explore whether the distinct volume and O atoms can influence the final structures.

To the best of our knowledge, the rigid organic ligands are extremely popular for construction of new POMOFs on account of their relatively fixed coordination modes in favor of target syntheses[6]. Among the various rigid ligands, 2,2-biimidazole has been viewed as a preferred one to construct POMOFs, which owns longer N⋯N distance and can induce binuclear metal clusters with ease[7]. In our previous work, we have discussed the influence of -CH_3 in bis(pyrazole) ligands on the architectures[8]. In this work, we still try to explore the effect of introduction of alkyl chain -$(CH_2)_nCH_3$ group to organic ligands on the structures of target compounds. Thus, in this work, 2,2-biimidazole (biz) and its derivative 5-butyl-2,2-biimidazole (bbiz) were selected as organic linkers to construct new POMOFs (Scheme 1). The bbiz ligand is firstly used in POM field to our knowledge. Furthermore, owing to the diverse coordination modes of Ag^+ ions and easy aggregation to form multi-nuclear Ag^+ clusters, we chose Ag^+ as the central metal ion[9].

On the basis of the aforementioned points, in this work, we chose Keggin/Ag^+/biz and Strandberg/Ag^+/bbiz systems to construct new POMOFs. Fortunately, we successfully obtained two new compounds under hydrothermal conditions: $[Ag_4(biz)_4][H_2P_2Mo_5O_{23}]\cdot 2H_2O$ (**1**) and $[Ag_4(bbiz)_4][HPW^{VI}_{10}W^{V}_{2}O_{40}]$ (**2**) (biz =2,2-biimidazole, bbiz =5-butyl-2,2-biimidazole). In addition, the electrochemical, photocatalytic and fluorescence properties of these two compounds have been studied.

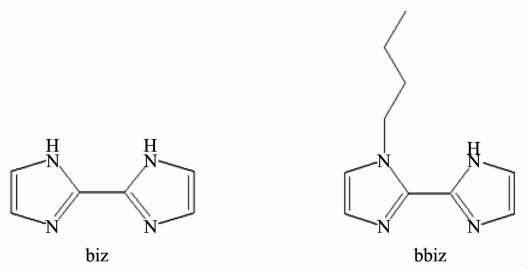

Scheme 1 2,2-biimidazole (biz) and its derivative 5-butyl-2,2-biimidazole (bbiz)

1 Experimental

1.1 Materials and Methods

All reagents were purchased from commercial sources and used without purification. Elemental analyses (C, H, and N) were performed on a Perkin-Elmer 2400 CHN elemental analyzer. The FTIR spectra were recorded from 4 000 ~400 cm^{-1} on a

Magna FTIR 560 Spectrometer with pressed KBr pellets. Electrochemical measurements were performed with a CHI 440 electrochemical workstation. A conventional three-electrode system was used. A saturated calomel electrode (SCE) was used as a reference electrode, and a Pt wire as a counter electrode. Chemically bulk-modified carbon-paste electrodes (CPEs) were used as the working electrodes. UV-Vis absorption spectra were obtained using a SP-1900 UV-Vis spectrophotometer.

1.2 Syntheses of compounds 1 and 2

$[Ag_4(biz)_4][H_2P_2Mo_5O_{23}]\cdot 2H_2O$ (**1**): A mixture of $Na_2MoO_4\cdot 2H_2O$ (0.134 g, 1.0 mmol), $AgNO_3$ (0.17 g, 1.0 mmol) and biz (0.2 g, 1.5 mmol) was dissolved in 10 mL of distilled water at room temperature. The suspension was stirred for 40 min in air and then pH value of the mixture was adjusted to about 1.3 with 1.0 mol·L^{-1} H_3PO_4. The suspension was transferred to a Teflon-lined stainless steel autoclave (20 mL) and kept under autogenous pressure at 160 ℃ for 3 days. After slow cooling (10 ℃·h^{-1}) to room temperature, yellow clavate crystals of **1** were obtained (45% yield based on Mo). Elemental analysis(%) calcd. for $C_{24}H_{30}Mo_5N_{16}Ag_4O_{25}P_2$ (1 915.71): C 15.04, H 1.46, N 11.7. Found: C 15.08, H 1.49, N 11.65.

$[Ag_4(bbiz)_4][HPW^{VI}_{10}W^{V}_{2}O_{40}]$ (**2**): The synthetic method was similar to that of compound **1**, except that $H_3PW_{12}O_{40}\cdot 13H_2O$ (0.08 g, 0.47 mmol) was used instead of $Na_2MoO_4\cdot 2H_2O$, while bbiz (0.015 g, 0.05 mmol) was used instead of biz. Brownness block crystals were filtered and washed with distilled water (47% yield based on W). Elemental analysis (%) calcd. for $C_{40}H_{56}Ag_4N_{16}O_{40}PW_{12}$ (4 069.54): C 11.79, H 1.37, N 5.5. Found: C 11.83, H 1.34, N 5.53.

1.3 X-ray crystallography

Crystallographic data for compounds **1** and **2** were collected on a Bruker Smart Apex Ⅱ diffractometer with Mo $K\alpha$(λ=0.071 073 nm) by using

Table 1　Crystal data and structure refinements for compounds 1 and 2

Complex	**1**	**2**
Empirical formula	$C_{24}H_{30}Ag_4Mo_5N_{16}O_{25}P_2$	$C_{40}H_{56}Ag_4N_{16}O_40PW_{12}$
Formula weight	1 915.71	4 069.54
Temperature / K	293(2)	296(2)
Crystal system	Monoclinic	Orthorhombic
Space group	$P2_1/c$	$Pbca$
a / nm	1.049 5(5)	1.568 99(9)
b / nm	2.724 7(5)	2.066 17(12)
c / nm	1.682 7(5)	2.280 50(14)
β / (°)	99.858(5)	90
V / nm^3	4.741(3)	7.392 9(8)
Z	4	4
D_c / (g·cm^{-3})	2.683	3.656
Absorption cofficient / mm^{-1}	3.061	19.736
F(000)	3 652	7 276.0
Crystal size / mm	0.23×0.21×0.18	0.17×0.16×0.15
θ range for data collection / (°)	1.97~28.17	1.79~25.00
Reflections collected / unique	29 292 / 11 645	29 292 / 11 645
R_{int}	0.026 7	0.085 4
Completeness / %	97.5	99.9
Goodness-of-fit on F^2	1.035	1.092
Final R^a indices ($I>2\sigma(I)$)	R_1=0.041 7, wR_2=0.107 4	R_1=0.068 2, wR_2=0.133 9
R^a indices (all data)	R_1=0.057 1, wR_2=0.115 2	R_1=0.103 5, wR_2=0.143 6

$^aR_1=\sum \| F_o \| - \| F_c \| / \sum | F_o |$; $wR_2=\{\sum[w(F_o^2-F_c^2)^2]/\sum[w(F_o^2)^2]\}^{1/2}$

an φ-ω scan mode at 293 K. All the structures were solved by direct methods and refined on F^2 by full-matrix least-squares methods using the SHELXTL package[10]. All the hydrogen atoms attached to carbon atoms were generated geometrically, while the hydrogen atoms attached to water molecules were not located but were included in the structure factor calculations. A summary of the crystallographic data and structural refinement for the title compounds are given in Table 1. Selected bond lengths and angles of **1** and **2** are listed in Table S1.

CCDC: 1027614, **1**; 1027615, **2**.

2 Results and discussion

2.1 Description of the structure

2.1.1 Crystal structure of compound **1**

Crystal structure analysis reveals that compound **1** is composed of four Ag^+ ions, four biz ligands, one $[P_2Mo_5O_{23}]^{6-}$ anion (abbreviated to P_2Mo_5) and two crystal water molecules, as shown in Fig.1. The P_2Mo_5 anion shows a classical Strandberg type with five distorted edge- and corner-sharing MoO_6 octahedra capped two PO_4 tetrahedra on each side. The bond valence sum calculations indicate that all the Mo atoms are in the +6 oxidation state and all the Ag atoms are in +1 oxidation state [11]. To balance the charge of the compound, two protons are added, then **1** is formulated as $[Ag_4(biz)_4][H_2P_2Mo_5O_{23}]\cdot 2H_2O$.

In compound **1**, there are four crystallographically independent Ag^+ ions (Ag1, Ag2, Ag3 and Ag4), which exhibit two coordination modes: (i) Both the Ag1 and Ag2 ions with T-type coordination geometries are three-coordinated by two N atoms (N3 and N7 for Ag1, N1 and N5 for Ag2) from two biz ligands and one Ag atom. (ii) The Ag3 and Ag4 ion adopts four-coordinated distorted seesaw coordination geometries, coordinated by two N atoms (N9 and N13 for Ag3, N11 and N19 for Ag4) from two biz ligands, one Ag ion and one terminal O atom (O14 for Ag3 and O19 for Ag4) from one P_2Mo_5 anion. The distance and angles around the Ag^+ ions are 0.211 1(4) ~0.214 5(3) nm for Ag-N, 0.283 9(7)~0.287 5(8) nm for Ag-Ag, 161.55 (14)° ~171.34 (15)° for N-Ag-N, 84.18(10)°~89.77(10)° for N-Ag-Ag. The bond lengths and angles are listed in Table S1.

The biz ligand in compound **1** shows a single coordination mode: each imidazole group offers one N donor to link two different Ag^+ ions. Thus, two kinds of bi-nuclear Ag^+ clusters are formed containing $[(Ag1)(Ag2)(biz)_2]^{2+}$ and $[(Ag3)(Ag4)(biz)_2]^{2+}$ clusters. Furthermore, the P_2Mo_5 anions provides two terminal oxygen atoms to link adjacent bi-nuclear $[(Ag3)(Ag4)(biz)_2]^{2+}$ clusters to form an infinite jagged 1D chain in a ABAB mode (Fig.2). The adjacent chains further built a 2D supramolecular layer through hydrogen bonding interactions, such as C24⋯O4 (0.310 6 nm)

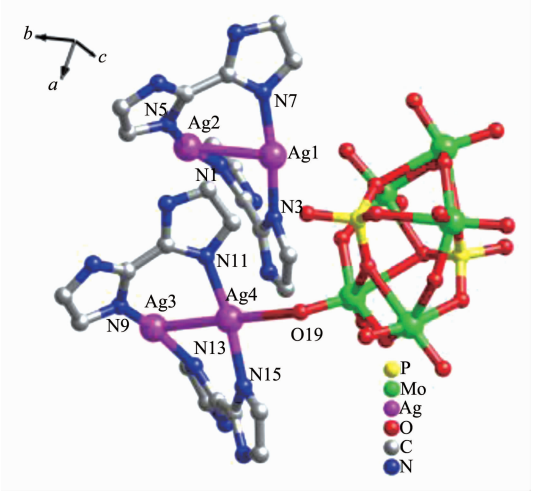

Hydrogen atoms and crystal water molecules are omitted for clarity

Fig.1 Ball and stick view of the asymmetric unit of **1**

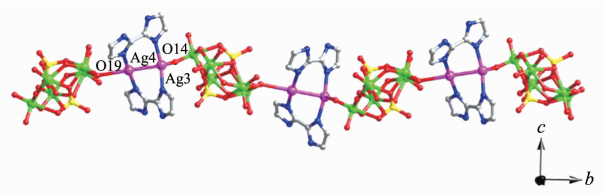

Fig.2　1D chain of compound **1** with the P_2Mo_5 anions and bi-nuclear $[(Ag3)(Ag4)(biz)_2]^{2+}$ clusters arranging alternately

shown in Fig.S1. The $[(Ag1)(Ag2)(biz)_2]^{2+}$ clusters acting as cationic complexes insert into adjacent 2D layers through hydrogen bonding interactions to stabilize the structure.

2.1.2　Crystal structure of compound **2**

Crystal structure analysis reveals that compound **2** consists of four Ag^+ ions, four bbiz ligands and one $[PW_{12}O_{40}]^{3-}$ anion (abbreviated to PW_{12}) (Fig.3). The PW_{12} presents a classical α-Keggin type anion. The central P atom is surrounded by a cube of eight O atoms with each site half-occupied[12]. The valence sum calculations show that two of the twelve W atoms are in +5 oxidation state and all the Ag atoms are in +1 oxidation state [11]. One proton is added to balance the charge of compound **2**, then **2** is formulated as $[Ag_4(bbiz)_4][HPW^{VI}_{10}W^{V}_{2}O_{40}]$. Under hydrothermal conditions, the organonitrogen species generally act not only as ligands but also as reductants, inducing the reduction of W in compound **2**[13].

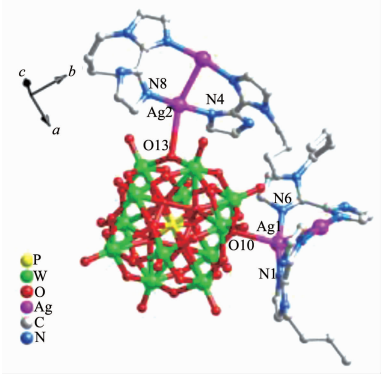

Hydrogen atoms and crystal water molecules are omitted for clarity

Fig.3　Ball and stick view of the asymmetric unit of **2**

There are two crystallographically independent Ag^+ ions (Ag1 and Ag2) in compound **2**. The Ag1 and Ag2 exhibit similar slightly distorted seesaw coordination geometries, coordinated by two nitrogen atoms (N1 and N6 for Ag1, N4 and N8 for Ag2) from two bbiz ligands, one bridging atom (O10 for Ag1 and O13 for Ag2) from one PW_{12} anion and one Ag atom. The distance and angles around the Ag^+ ions are 0.206 4(9)~0.213 7(8) nm for Ag-N, 0.282 8(11) nm for Ag-Ag, 170.9(3)°~174.4(3)° for N-Ag-N, 85.4(2)°~87.4(2)° for N-Ag-Ag. The bond lengths and angles are listed in Table S1.

The bbiz shows the same coordination mode with that in compound **1**. There also exists a bi-nuclear $[(Ag1)(Ag2)(bbiz)_2]^{2+}$ cluster. Each PW_{12} anion offers four bridging O atoms (two O10 and two O13) to link four bi-nuclear Ag^+ clusters to construct a 2D layer of compound **2** (Fig.4).

2.1.3　Effect of different anions on structures of **1** and **2**

We chose biz and P_2Mo_5 for construction of **1** and chose bbiz and PW_{12} for **2**, in order to explore whether the butyl group in ligands and different anions have influences on the structures[14]. Though the butyl group shows a few hydrogen interactions, it has no obvious effect on the structures. However, the different anions

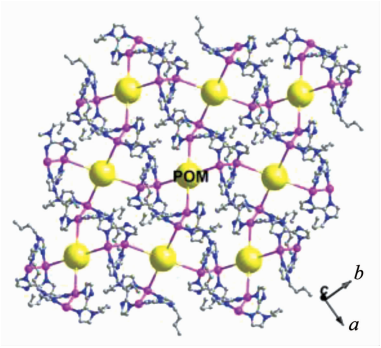

Fig.4 2D layer of compound **2** (the biggest balls: Keggin anions)

(P_2Mo_5 for **1** and PW_{12} for **2**) really induce distinct structures of **1** and **2**. In compound **1**, the P_2Mo_5 anion owns a smaller volume. Thus, in order to reduce the repulsions between bi-nuclear $[(Ag3)(Ag4)(biz)_2]^{2+}$ clusters, the P_2Mo_5 anion only offers two symmetrical terminal O atoms to link two bi-nuclear clusters (Fig. S2a). But the PW_{12} anion in **2** owing to big volume can link four bi-nuclear Ag^+ clusters by providing four bridging O atoms (Fig.S2b). If the P_2Mo_5 anion also supplies its two bridging O atoms instead of terminal ones, the repulsions of bi-nuclear Ag^+ clusters will increase. Furthermore, the coordination number of P_2Mo_5 is also less than that of PW_{12}. Thus, the different anions play a key role on construction of the structures of **1** and **2**.

2.2 FTIR Spectra

The IR spectra of compounds **1** and **2** are shown in Fig.S3. In the spectrum of **1**, characteristic bands at 785, 862, 957 and 1 060 cm^{-1} correspond to ν(Mo-O_c-Mo), ν(Mo-O_b-Mo), ν (Mo=O_d) and ν(P-O) of the P_2Mo_5 anion, respectively [4c]. In the spectrum of **2**, 1 072, 977, 888, 805 are attributed to the ν(P-Oa), ν(W-Od) and ν(W-Ob-W) of the PW_{12} anion, respectively[15]. Bands in the regions of 1 563~1 245 cm^{-1} for **1** and 1 537~1 168 cm^{-1} for **2** are attributed to the biz and bbiz ligands, respectively.

2.3 Electrochemical properties

The electrochemical behaviors of **1** and **2** were investigated with 1- and 2-modified CPE (1- and 2-CPE). The cyclic voltammograms for the CPEs in 0.1 $mol\cdot L^{-1}$ H_2SO_4+0.5 $mol\cdot L^{-1}$ Na_2SO_4 aqueous solution at different scan rates are presented in Fig.5. Three reversible redox peaks appear in the potential range from +460 to −250 mV for 1-CPE, corresponding to three consecutive two-electron processes of P_2Mo_5. The mean peak potentials ($E_{1/2}$=(E_{pa}+E_{pc})/2) (scan rate: 250 $mV\cdot s^{-1}$) are 224 (Ⅰ-Ⅰ′), 39 (Ⅱ-Ⅱ′) and -165 (Ⅲ-Ⅲ′) mV for the 1-CPE [16]. The cyclic voltammograms of 2-CPE at different scan rates are presented in the potential range of +100 to −780 mV. There also exist three reversible redox peaks Ⅰ-Ⅰ′, Ⅱ-Ⅱ′ and Ⅲ-Ⅲ′ with the mean peak potentials ($E_{1/2}$=(E_{pa}+E_{pc})/2) of

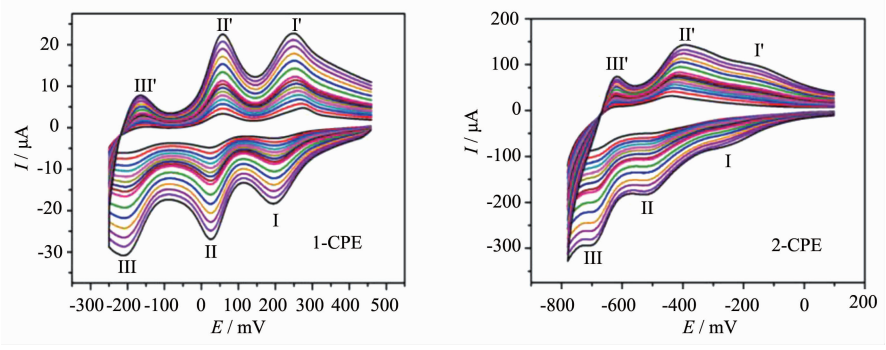

From inner to outer: 40, 60, 80, 100, 120, 140, 160, 180, 200, 250, 300, 350, 400, 450 and 500 $mV\cdot s^{-1}$, respectively

Fig.5 Cyclic voltammograms of the 1- and 2-CPEs in 0.1$mol\cdot L^{-1}$ H_2SO_4+ 0.5 $mol\cdot L^{-1}$ Na_2SO_4 aqueous solution at different scan rates

−178, −466, −661 mV (scan rate: 250 mV·s^{-1}). Redox peaks Ⅰ-Ⅰ′ and Ⅱ-Ⅱ′ correspond to two consecutive one-electron processes, while Ⅲ-Ⅲ′ corresponds to a two-electron process of PW_{12}[8]. The peak potentials of cyclic voltammograms for the CPEs change gradually following the scan rates from 40 to 500 mV·s^{-1}: the cathodic peak potentials shift toward the negative direction and the corresponding anodic peak potentials to the positive direction with increasing scan rates. When the scan rate is up to 500 mV·s^{-1}, the peak currents are proportional to the scan rates, which shows that the redox process of the 1- and 2-CPEs are surface-confined (Fig.S4).

Fig.6 shows cyclic voltammograms for the electrocatalytic reduction of hydrogen peroxide at 1- and 2-CPEs in 0.1 mol·L^{-1} H_2SO_4 + 0.5 mol·L^{-1} Na_2SO_4 aqueous solution. It can be clearly seen that with addition of H_2O_2, all three reduction peak currents of 1- and 2-CPEs gradually increase, while the corresponding oxidation peak currents decrease. These phenomena indicate that the three reductive species of P_2Mo_5 in **1** and PW_{12} in **2** all possess electrocatalytic activities for the reduction of hydrogen peroxide. In a word, compounds **1** and **2** may be used as good potential electrocatalysts.

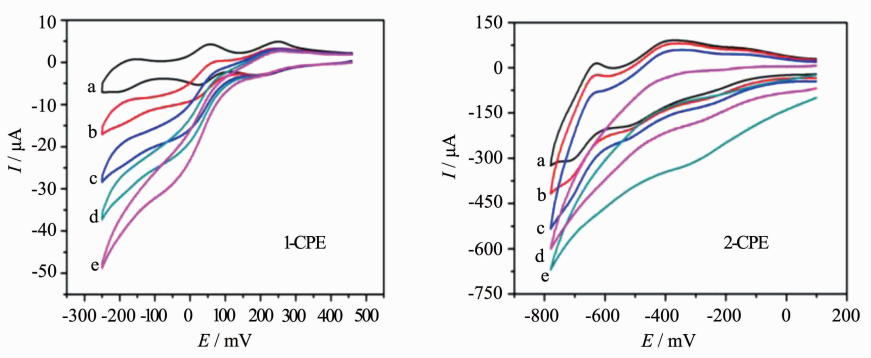

Scan rate: 200 mV·s^{-1}

Fig.6　Cyclic voltammograms of the 1- and 2-CPEs in 0.1 mol·L^{-1} H_2SO_4+0.5 mol·L^{-1} Na_2SO_4 aqueous solution containing 0 (a), 2 (b), 4 (c), 6 (d) and 8 (e) mmol·L^{-1} H_2O_2

2.4 Photocatalytic activity

Some POM-based compounds exhibit photocatalitic activities to degrade organic dyes [17]. Therefore, the photocatalytic activities of compounds **1** and **2** were investigated by the degradation of methylene blue(MB) and Rhodamine-B(RhB) solution under UV irradiation, as shown in Fig.7 and Fig.8. In the process of photocatalysis, 100 mg title compounds was suspended in 0.02 mmol·L^{-1} MB or RhB aqueous solution 250 mL and magnetically stirred for about 10 min to ensure the equilibrium in the dark. Every 20 min, the sample of 5 mL was taken out, which was

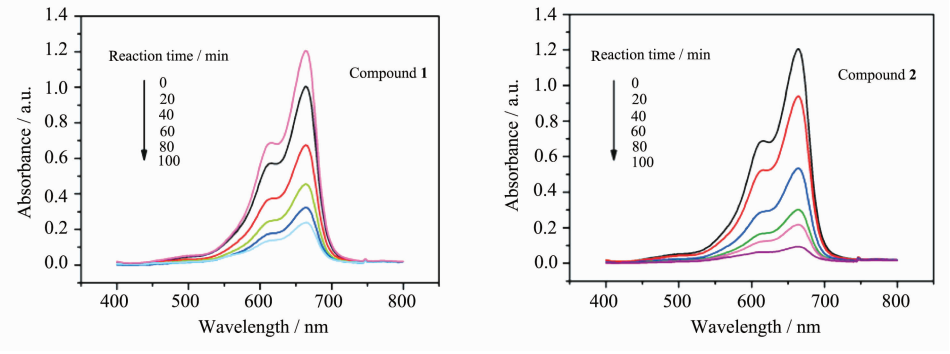

Fig.7　Absorption spectra of the MB solution during the decomposition reaction under UV irradiation in the presence of compounds **1** and **2**

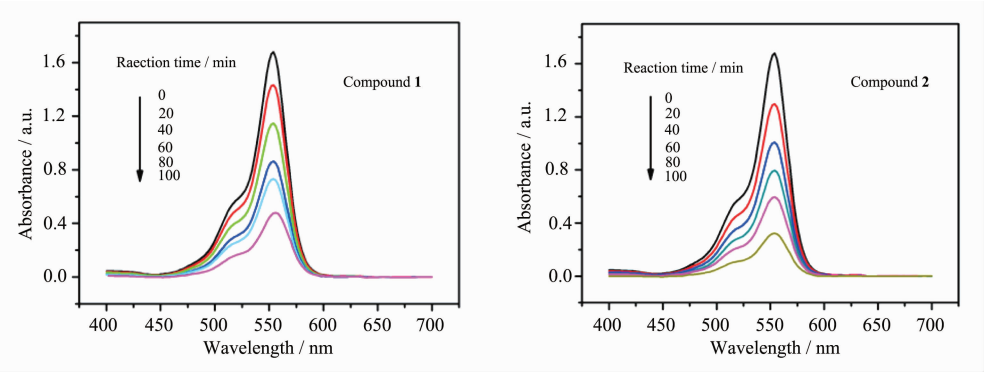

Fig.8 Absorption spectra of the RhB solution during the decomposition reaction under UV irradiation in the presence of compounds **1** and **2**

obtained for analysis by UV-Visible spectroscopy. The absorption peaks of MB photocatalyzed by **1** and **2** decreased obviously with increasing of reaction time and the conversions of MB are 80.99% for compound **1** and 93.38% for **2** after 100 min (Fig.S5a). Fig.8 and Fig.S5b show that the conversions of RhB are 72.46% for **1** and 80.83% for **2**, respectively. This results show that the title compounds own good photocatalytic activities for the degradation of MB and RhB, especially compound **2**.

2.5 Fluorescent properties

In this work, the fluorescent properties of the title compounds in the solid state at room temperature were investigated. Emission spectra of **1** and **2** are shown in Fig. S6. Two prominent emission peaks are observed at about 417 and 467 nm for **1**, 414 and 466 nm for **2** (excitation at 340 nm). The emission peak would be assigned to ligand-to-metal charge transfer (LMCT) [18]. These observations exhibit that the title compounds may be candidates for photoluminescence materials.

3 Conclusions

In summary, by using biz and bbiz ligands two new POM-based compounds have been successfully synthesized. In compound **1**, the bi-nuclear $[Ag_2(biz)_2]^{2+}$ clusters are linked by P_2Mo_5 anions to form a 1D chain. Compound **2** displays a 2D layer constructed by tetra-dentate PW_{12} anions and bi-nuclear $[Ag_2(bbiz)_2]^{2+}$ clusters. The different POM anions induce distinct structures of **1** and **2**. Though the butyl group exhibits no obvious effect, further study on its influence on other structures is underway.

Acknowledgements: Financial supports of this research by the National Natural Science Foundation of China (No. 21101015, 21471021 and 21201021), Program of Innovative Research Team in University of Liaoning Province (No. LT2012020) and Talent-supporting Program Foundation of Education Office of Liaoning Province (No. LJQ2012097).

Supporting information is available at http://www.wjhxxb.cn

References:

[1] (a) Manna K, Zhang T, Carboni M, et al. *J. Am. Chem. Soc.*, **2014**,**136**(38):13182-13185;
(b) Ahmed A, Forster M, Clowes R, et al. *Chem. Commun.*, **2014**,**50**:14314-14316;
(c) Phang W J, Lee W R, Yoo K, et al. *Angew. Chem. Int. Ed.*, **2014**,**53**(32):8383-8387
[2] (a) Kikukawa Y J, Kuroda Y, Yamaguchi K, et al. *Angew. Chem. Int. Ed.*, **2012**,**124**(10):2484-2487;
(b) Miao H, Xu X, Ju W W, et al. *Inorg. Chem.*, **2014**,**53**(6): 2757-2759;
(c) Zhang Z Y, Lin Q P, Kurunthu D, et al. *J. Am. Chem. Soc.*, **2011**,**133**(18):6934-6937;
(d) Fu H, Qin C, Lu Y, et al. *Angew. Chem. Int. Ed.*, **2012**,**51**:7985-7989
(e) Wang X L, Bi Y F, Chen B K, et al. *Inorg. Chem.*, **2008**, **47**(7):2442-2448
[3] (a) Balula S S, Cunha-Silva L, Santos I C M S, et al. *New J. Chem.*, **2013**,**37**:2341-2350;
(b) Tian A X, Ying J, Peng J, et al. *Inorg. Chem.*, **2009**,**48**(1): 100-110;
(c) Wang X L, Li N, Tian A X, et al. *Inorg. Chem.*, **2014**,**53**

(14):7118-7129

[4] (a) Nagazi, I, Haddad A. *J. Cluster Sci*., **2014**,**25**:627-638

(b) Jin H J, Zhou B B, Yu Y, et al. *Chem. Eng. Commun.*, **2011**,**13**,585-590

(c) Shi J, Wang C X, Yu K, et al. *J. Coord. Chem*., **2014**,**67** (13):2229-2237

[5] Li Z L, Wang Y, Zhang L C, et al. *Dalton Trans*., **2014**,**43**: 5840-5846

[6] (a) Wang L M, Wang Y, Fan Y, et al. *Chem. Eng. Commun.*, **2014**,**16**:430-440

(b) Yang H X, Guo S P, Tao J, et al. *Cryst. Growth Des*., **2009**,**9**:4735-4744

(c) Sun J W, Li M T, Sha J Q, et al. *Chem. Eng. Commun*., **2013**,**15**:10584-10589

[7] (a) Wang Y, Zhang L C, Zhu Z M, et al. *Transition Met. Chem*., **2011**,**36**:261-267

(b) Xu Y L, Zhou B B, Su Z H, et al. *J. Coord. Chem.*, **2011**,**64**:3670-3678

[8] Tian A X, Yang Y, Ying J, et al. *Dalton Trans*., **2014**,**43**: 8405-8413

[9] (a) Wang L, Yang W T, Zhu W, et al. *Inorg. Chem.*, **2014**, **53** (21):11584-11588

(b) Zhou K, Qin C, Wang X L, et al. *Chem. Eng. Commun.*, **2014**,**16**:10376-10379

(c) Li M T, Sha J Q, Zong X M, et al. *Cryst. Growth Des*., **2014**,**14**(6):2794-2802

[10](a) Sheldrick G M. *SHELXS*-97, *Program for Crystal Structure Solution*. University of Göttingen, Germany, **1997**.

(b) Sheldrick G M. *Acta Crystallogr. Sect. A*, **2008**,**64**:112

[11]Brown I D, Altermatt D. *Acta Crystallogr*., Sect. B, **1985**,**41**: 244-247

[12]Jr Evans H T, Popev M T. *Inorg. Chem*., **1984**,**23**:501-504

[13]Liu C M, Zhang D Q, Zhu D B. *Cryst. Growth Des*., **2006**,**6**: 524-529

[14](a) Wang X L, Li N, Tian A X, et al. *Dalton Trans*., **2013**, **42**:14856-14865

(b) Zhai Q G, Wu X Y, Chen S M, et al. *Inorg. Chem*., **2007**,**46**:5046-5058

(c) Zhang P P, Peng J, Pang H J, et al. *Chem. Eng. Commun*., **2011**,**13**:3832-3841

[15](a) Dobrick M S, Jansen M. *Eur. J. Inorg. Chem.*, **2006**,**22**: 4498-4502

(b) Liu H Y, Wu H, Yang J, et al. *Cryst. Growth Des*., **2011**,**11**(5):1786-1797

[16]Guo H X, Li X Z, Weng W. *Inorg. Chem. Commun.*, **2010**,**13**:909-913

[17](a) Li T H, Li Q G, Yan J, et al. *Dalton Trans*., **2014**,**43**: 9061-9069

(b) Tian A X, Yang Y, Sun N, et al. *J. Coord. Chem.*, **2014**, **67**(9):1550-1561

[18]Wang X, Peng J, Liu M G, et al. *Chem. Eng. Commun*., **2012**,**14**:3220-3226